· Article · Advances in Polar Science
doi: 10.12429/j.advps.2022.0010 September 2023 Vol. 34 No. 3: 177-189

Assessment of Greenland surface melt algorithms based on DMSP and SMOS data

LI Qian[1,2], WANG Che[1*], ZHANG Tong[3], CHENG Wei[4] & DING Minghu[2]

[1] State Key Laboratory of Urban Environmental Processes and Digital Simulation, Capital Normal University, Beijing 100048, China;
[2] State Key Laboratory of Severe Weather, Chinese Academy of Meteorological Sciences, Beijing 100081, China;
[3] State Key Laboratory of Earth Surface Processes and Resource Ecology, Beijing Normal University, Beijing 100875, China;
[4] Beijing Institute of Applied Meteorology, Beijing 100029, China

Received 22 July 2022; accepted 28 November 2022; published online 30 June 2023

Abstract Satellite-borne microwave radiometers provide essential measurements to study the surface melt state of ice sheets. Therefore, selecting suitable microwave radiometer data is critical to characterize the spatial distribution of surface melt. In this study, we investigated the Greenland Ice Sheet and evaluated the usefulness, as climate indicators, of data acquired by microwave radiometers onboard the F17 satellite of the United States of America Defense Meteorological Satellite Program (DMSP) and the Soil Moisture and Ocean Salinity (SMOS) satellite of the European Space Agency. First, surface melt was simulated using the DMSP dataset as input for a brightness temperature threshold algorithm, the Microwave Emission Model of Layered Snowpacks (MEMLS2), and the SMOS dataset as input for the L-band Specific MEMLS (LS-MEMLS). For accuracy evaluation, the simulation results were then compared with surface melt estimates derived from air temperature measurements at Automatic Weather Stations and from ice surface temperature measurements from the Moderate Resolution Imaging Spectroradiometer (MODIS) satellite-borne instrument. Our results show that global (over Greenland) MEMLS2 simulation performance (overall accuracy 83%) was higher than that of LS-MEMLS (overall accuracy 78%). However, in southeastern Greenland, MEMLS2 omission error was markedly higher than that of LS-MEMLS, whereas LS-MEMLS could detect longer-lasting surface melt than MEMLS2. This analysis showed that DMSP-based surface melt simulations are more accurate than SMOS-based simulations, thereby providing a data selection reference for surface melt studies of the Greenland Ice Sheet.

Keywords **Greenland Ice Sheet, surface melt, microwave radiometer, MEMLS2, LS-MEMLS**

Citation: Li Q, Wang C, Zhang T, et al. Assessment of Greenland surface melt algorithms based on DMSP and SMOS data. Adv Polar Sci, 2023, 34(3): 177-189, doi: 10.12429/j.advps.2022.0010

1 Introduction

Greenland is covered by the second largest continental ice sheet after Antarctica, which would cause, if it melted completely, an approximate sea-level rise of 7 m (Gregory and Huybrechts, 2006). Recently, severe Greenland Ice Sheet mass loss has caused an acceleration in global sea-level rise. For example, Smith et al. (2020) measured a Greenland mass loss rate of approximately 200 $Gt \cdot a^{-1}$ in 2003–2019, which corresponds to a sea-level rise of 8.9 mm. Greenland Ice Sheet mass loss occurs through glacial discharge and surface mass loss (Rignot et al., 2008). Surface mass loss is mainly caused by the runoff of surface meltwater into the ocean (van den Broeke et al., 2017). Historically, glacial discharge was the main mass loss

* Corresponding author, ORCID: 0009-0002-0379-227X, E-mail: 6697@cnu.edu.cn

process. Rignot et al. (2008), for example, reported that glacial discharge dominated Greenland Ice Sheet mass loss from 1958–2007. However, the contribution of surface mass loss has gradually increased. For example, van den Broeke et al. (2016) estimated a contribution of surface mass loss approximately 60% to the total Greenland mass loss in 1991–2015. Therefore, studying surface melt on the Greenland Ice Sheet is important to understand and predict sea-level rise in the current climate-change context.

Currently, remote sensing data used for surface melt study of polar ice sheets are mainly acquired by optical imagers, Synthetic Aperture Radars (SAR), microwave scatterometers and microwave radiometers. Hall et al. (2013) estimated daily values of the Greenland Ice Sheet surface melt from 2000–2012, with a spatial resolution of 780 m, using ice surface temperature data from the Moderate Resolution Imaging Spectroradiometer (MODIS). Liang et al. (2021) used the Google Earth Engine to extract monthly values of the Antarctic Ice Sheet melt from 2015–2019 from SAR images, with a spatial resolution of 40 m, by applying the orbit normalization technique. Although optical and SAR images provide high-resolution melt estimates, optical image quality is strongly affected by clouds, while SAR images cannot provide dynamic monitoring of an entire ice sheet. Conversely, microwave remote sensing provides continuous day- and nighttime observations in any weather, thus it allows for dynamic large-scale monitoring of the Greenland Ice Sheet (Wang, 2013). Among microwave instruments, scatterometers require more data pre-processing and more complicated melt detection methods than radiometers. Therefore, radiometer-based melt detection methods are more mature (Wang, 2013).

Since the late 1970s, continuous satellite-borne microwave radiometer observations have been available for polar ice sheet surface melt studies. They were acquired successively by the Scanning Multichannel Microwave Radiometer (SMMR) onboard the Nimbus-7 meteorological satellite of the United States of America (U.S.) National Aeronautics and Space Administration (NASA), providing data from 1978–1987 (Joshi et al., 2001; Tedesco, 2009); by two series of sensors onboard satellites of the U.S. Defense Meteorological Satellite Program (DMSP): the Special Sensor Microwave/Imager (SSM/I), since 1987, and the Special Sensor Microwave Imager/Sounder (SSMI/S), since 2003 (Colosio et al., 2021); and by the Microwave Imaging Radiometer using Aperture Synthesis (MIRAS) instrument onboard the Soil Moisture and Ocean Salinity (SMOS) satellite of the European Space Agency (Houtz et al. 2021), since 2010.

For DMSP satellite, the most common radiometer observation frequencies for surface melt studies are 19 GHz in the K-band, and 37 GHz in the Ka-band (Colosio et al., 2021). Corresponding surface melt analysis methods include edge detection or brightness temperature threshold identification (Tedesco, 2009). Abdalati and Steffen (1995) proposed a "cross-polarized gradient ratio threshold" method (XPGR) using horizontally polarized data at 19 GHz and vertically polarized data at 37 GHz from the SSM/I sensors. Joshi et al. (2001) developed a Gaussian edge detection algorithm using vertically polarized data at 18 GHz from SMMR on Nimbus-7 and vertically polarized data at 19 GHz from the SSM/I sensors. Tedesco (2009) proposed a brightness temperature threshold snowmelt calculation method (hereafter MEMLS2) by applying the Microwave Emission Model of Layered Snowpacks (MEMLS) to SMMR and SSM/I horizontally polarized data at 19 GHz, assuming a wet snow layer thickness of 5 cm and a liquid water content set to 0.2%. More recently, SMOS data have also been applied to surface melt studies. For example, Houtz et al. (2019) quantified surface melt with the L-band Specific Microwave Emission Model of Layered Snowpacks (LS-MEMLS); they analyzed SMOS L-band data at 1.4 GHz to calculate liquid water content at the "Swiss Camp" research site in the West Greenland ablation zone.

To assess the potential usefulness as climate indicators of surface melt simulations using DMSP and SMOS data, this study evaluates the accuracy of the DMSP-based MEMLS2 and SMOS-based LS-MEMLS algorithms, first by comparing the results with surface melt estimates derived from automatic weather station (AWS) air temperatures and from MODIS ice surface temperatures, then by cross-comparing the algorithms. The analysis focuses on the annual ablation season (June–August) over a 10-year study period, from 2011–2020. The analysis flowchart is illustrated in Figure 1.

2 Data and methods

2.1 Data

2.1.1 DMSP-F17 data

The seventeenth "flight unit" of the DMSP Block 5D series (DSMP-F17) has been operational since 2006 with high orbital stability. Ka-band data at 37 GHz are acquired by the SSMI/S instrument in horizontal and vertical polarization, with a spatial resolution of 25 km and a revisit period of one day. In this study, we extracted brightness temperature data from the MEaSUREs Calibrated Enhanced-Resolution Passive Microwave Daily EASE-Grid 2.0 Brightness Temperature ESDR, Version 1 dataset, part of the NASA Making Earth System Data Records for Use in Research Environments (MEaSUREs) project (Brodzik et al., 2016), acquired annually during the ablation season (June–August) over the 2011–2020 study period, and available from the U.S. National Snow and Ice Data Center (NSIDC, https://nsidc.org/data/nsidc-0630/versions/1). Selected DMSP data were then used as input for the MEMLS2

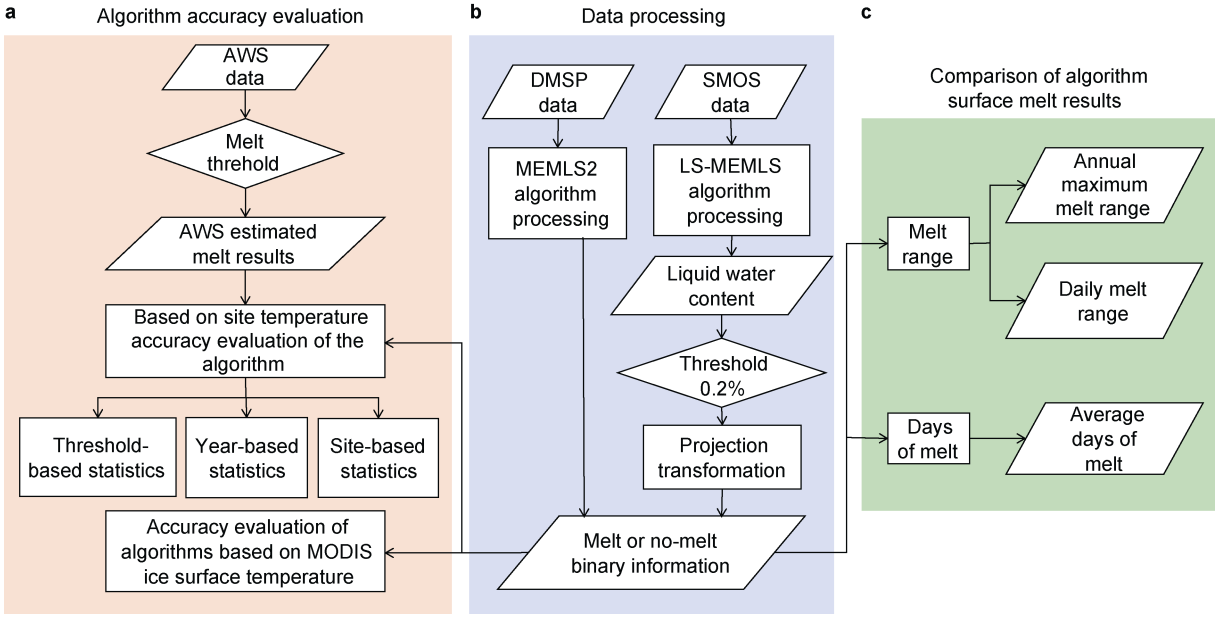

Figure 1 Algorithm assessment flowchart including accuracy evaluation (**a**), DMSP and SMOS satellite data processing by MEMLS2 and LS-MEMLS, respectively (**b**), and cross-comparison between the algorithms (**c**).

algorithm to characterize global surface melt in Greenland.

2.1.2 SMOS data

The SMOS satellite has been operational since 2010 and provides global measurements of surface soil moisture and sea surface salinity. This study selects SMOS level 3 bright temperature data for the ablation period (June to August) from 2011 to 2020 and uses the LS-MEMLS algorithm to obtain surface melt for the whole Greenland for the last decade. The SMOS satellite is in a sun-synchronous orbit at an altitude of 758 km (period of 100 min) and an inclination of 98.45°, corresponding to approximately 14.4 orbits data, covering the Earth twice a day (28 ascending and descending orbits segments). L-band data at 1.4 GHz are acquired in horizontal and vertical polarization, with a spatial resolution of 25 km, a revisit period of 1 d, and 14 incidence angles, although brightness temperatures are not measured at all angles. Similar to DMSP data, we extracted SMOS level 3 brightness temperature data (Al Bitar et al., 2017) acquired annually during the ablation season over the study period, available from the Centre Aval de Traitement des Données SMOS (https://www.catds.fr/sipad/). The SMOS data were used as input for the LS-MEMLS algorithm to characterize global surface melt in Greenland over the study period.

2.1.3 Evaluation data

Because no direct surface melt measurements are available for the Greenland Ice Sheet, surface melt can only be evaluated using temperature data (Tedesco, 2009). In this study, surface melt estimates from air temperature data measured at 23 AWSs (daily average at each station) and from MODIS ice surface temperature data were selected for algorithm evaluation. The AWSs are part of the Greenland Climate Network (GC-Net) (Steffen et al., 1996) and of the Programme for Monitoring of the Greenland Ice Sheet (PROMICE) (Table 1). MODIS ice surface temperature data were extracted from the “Multilayer Greenland Ice

Table 1 Locations of the automatic weather stations used in this study

Dataset	Site	Latitude/(°N)	Longitude/(°W)	Elevation/m
GC-Net	NASA-U	73.84	49.50	2369
	GITS	77.14	61.04	1887
	Humboldt	78.53	56.83	1995
	Summit	72.58	38.50	3254
	TUNU-N	78.02	33.99	2113
	DYE-2	66.48	46.28	2165
	Saddle	66.00	44.50	2559
	South Dome	63.15	44.82	2922
	NASA-E	75.00	30.00	2631

Continued

Dataset	Site	Latitude/(°N)	Longitude/(°W)	Elevation/m
GC-Net	NASA-SE	66.48	42.50	2425
	Peterman ELA	80.08	58.07	965
	NEEM	77.50	50.87	2454
PROMICE	KPC_U	79.83	25.17	870
	EGP	75.62	35.97	2660
	TAS_L	65.64	38.90	250
	TAS_U	65.70	38.87	570
	TAS_A	65.78	38.90	890
	NUK_U	64.51	49.27	1120
	KAN_M	67.07	48.84	1270
	KAN_U	67.00	47.03	1840
	UPE_L	72.89	54.30	220
	UPE_U	72.89	53.58	940
	CEN	77.13	61.03	1880

Surface Temperature, Surface Albedo, and Water Vapor from MODIS, Version 1" dataset (Hall and DiGirolamo, 2019), also available from the NSIDC (https://nsidc.org/data/modgrnld/versions/1). Radiative forcing from incoming solar radiation can cause melt to occur even for air temperatures below 0 °C. For this reason, three melt thresholds: 0 °C, –1 °C, and –2 °C were set for AWS air temperatures in this study (Tedesco, 2009; Colosio et al. 2021). For MODIS ice surface temperature, the melt threshold was set to –1 °C (Hall and DiGirolamo, 2019). Greenland basin delineation (Figure 2) was derived from the MODIS ice surface temperature product.

2.2 Methodology

2.2.1 Brightness temperature threshold methods

To determine the surface melt status of an ice sheet, several algorithms have been developed using DMSP satellite data as input, including edge detection and brightness temperature threshold methods (Tedesco, 2009). Briefly, edge detection algorithms consider that melt occurrence corresponds to the fastest brightness temperature variations (Wang, 2013). Alternately, brightness temperature threshold algorithms identify melt occurrence when brightness temperature exceeds a specific threshold value (Wang, 2013). Methods based on brightness temperature thresholds, extensively studied, are more refined and mature than edge detection algorithms. Therefore, the brightness temperature threshold method based on DMSP is mainly used in this study. The sensitivity of brightness temperature threshold methods to liquid water content in snow depends on the threshold: Methods with high thresholds show lower sensitivity, whereas methods with low thresholds are more sensitive (Tedesco et al., 2007; Tedesco, 2009). Several brightness temperature threshold methods (including those described in Table 2) were evaluated in previous studies. For example, Tedesco (2009) evaluated the algorithms defined in Table 2 by comparing their output with surface melt estimates from AWS air

Figure 2 Topographic map of Greenland showing AWS locations (black dots) and boundaries (gray lines) of the north, northwest, northeast, west-central, east-central, southwest, southeast, and south Greenland basins.

Table 2 Description of brightness temperature threshold methods used in previous studies

Algorithm	Formula	Reference
ALA	$T_c=T_{winter}\times\alpha+T_{wet\_snow}\times(1-\alpha)$, T_c is the bright temperature threshold, T_{winter} is the average winter bright temperature, T_{wet_snow} is the wet snow bright temperature (273 K), α is the mixing factor (0.47), mainly for the wet snow layer thickness of 4.7 cm and liquid water content of 1%.	Aschraft and Long, 2006
M+3s	$T_c=T_{winter}+\Delta T$, T_c is the bright temperature threshold, T_{winter} is the mean bright temperature in winter, $\Delta T=3\sigma$, σ is the standard deviation of bright temperature in winter.	Torinesi et al., 2003
M+30K	$T_c=T_{winter}+\Delta T$, T_c is the bright temperature threshold, T_{winter} is the average bright temperature in winter, ΔT=30 K.	Jay Zwally and Fiegles, 1994
245K	T_c=245 K, T_c is the bright temperature threshold, mainly for melt with liquid water content of 1% or more.	Tedesco et al., 2007
MEMLS1	$T_c=0.8T_{winter}+58$, T_c is the bright temperature threshold, T_{winter} is the average bright temperature in winter, mainly for a wet snow layer thickness of 5 cm and liquid water content of 0.1%.	Tedesco, 2009
MEMLS2	$T_c=0.48T_{winter}+128$, T_c is the bright temperature threshold, T_{winter} is the average bright temperature in winter, mainly for a wet snow layer thickness of 5 cm and liquid water content of 0.2%.	Tedesco, 2009

temperature; they reported that the ALA and 245K algorithms underestimated surface melt, whereas the M+3s and MEMLS1 overestimated surface melt, and only the MEMLS2 and M+30K algorithms were in good agreement with the comparison data. Colosio et al. (2021) evaluated the M+30K, M+35K, M+40K, 245K, and MEMLS2 algorithms by comparing with AWS air temperature data and with simulations from the Modèle Atmosphérique Régional (or MAR, for regional atmospheric model); their results showed that MEMLS2 is the most suitable algorithm for Greenland surface melt simulations.

Therefore, in this study, the MEMLS2 algorithm (Tedesco, 2009) was selected and applied to DMSP data to detect the Greenland Ice Sheet surface melt. The algorithm is derived from the MEMLS model with fixed parameters: The wet snow layer thickness is set to 5 cm and the liquid water content threshold (0.2%). The algorithm is a linear function of the winter brightness temperature, expressed as (Tedesco, 2009):

$$T_c = \gamma T_{winter} + \omega, \quad (1)$$

where T_{winter} is the average winter brightness temperature, $\gamma = 0.48$, and ω=128 K.

2.2.2 The LS-MEMLS method

Houtz et al. (2019) proposed a new method using the LS-MEMLS model to simulate surface melt from L-band microwave radiometer data. This method not only evaluates the state of the ice surface (melted or not) but also provides estimates of the liquid water content on the ice sheet surface. Therefore, it is more appropriate for ice sheet surface mass loss estimation than brightness temperature threshold methods. Because the MIRAS instrument onboard SMOS operates in the L-band at 1.4 GHz, the LS-MEMLS method was selected in this study to analyze the SMOS data. The basis of this method, the LS-MEMLS model, assumes the existence of seasonal snowpacks above a glacial ice sheet divided into an upper layer composed of wet snow and a lower layer with dry snow. First, the surface brightness temperature (at the bottom of the atmosphere) is simulated from known humidity and density values. Second, the loss function between the simulated and measured (by satellite-borne instruments) brightness temperatures is calculated. The final simulated humidity and density values in snowpacks on the ice sheet are obtained by minimizing the loss function (Houtz et al., 2019, 2021). Simulated brightness temperature in the LS-MEMLS model is expressed as Houtz et al. (2019, 2021):

$$T_{B,sim}^{p,\theta_j}(w_S, \rho_S) = LSMEMLS(w_S, \rho_S), \quad (2)$$

where $T_{B,sim}^{p,\theta_j}(w_S, \rho_S)$ is the simulated brightness temperature at the bottom of the atmosphere; w_s is the wet snow layer humidity, with values within 0–1 $m^3 \cdot m^{-3}$; ρ_s is the wet snow layer density, with values within 0.15–0.9 $g \cdot cm^{-3}$; $\rho = \{H,V\}$, ρ indicates the horizontal (H) or vertical (V) polarization mode; and θ_j is the incidence angle, with 14 possible values for SMOS measurements: 13 values within 2.5°–62.5° (with an interval of 5°) and 40°. Details of the model are given in Houtz et al. (2019). The loss function is nominally expressed as Houtz et al. (2019, 2021):

$$CF(w_S, \rho_S) = \sum_{j=1,\ \rho=\{H,V\}}^{n} \frac{\left[T_B^{p,\theta_j} - T_{B,sim}^{p,\theta_j}(w_S, \rho_S)\right]^2}{(\sigma_{T_B^{p,\theta_j}})^2 + \sigma_{SMOS}^2}, \quad (3)$$

where T_B^{p,θ_j} is the SMOS measured brightness temperature (in K); $\sigma_{T_B^{p,\theta_j}}$ is the angular standard deviation provided in the SMOS dataset; σ_{SMOS} = 3 K is the instrumental uncertainty; and $CF(w_S, \rho_S)$ represents the

loss (or cost) function. The liquid water content simulation result is obtained when the loss function is minimized.

The output of the MEMLS2 algorithm is a binary result on the occurrence or absence of melt. However, the LS-MEMLS algorithm output is a liquid water content value, thus binary information on the occurrence/absence of melt must be derived from this result to compare with MEMLS2. Assuming a wet snow layer thickness of 5 cm, melt is detected by the MEMLS2 algorithm when the liquid water content is 0.2% or more (Tedesco, 2009); in this study, a wet snow layer thickness of 10 cm was defined for liquid water content calculations in the LS-MEMLS algorithm (Houtz et al., 2021). To compare results from both algorithms, a liquid water content of 0.2% was set as the melt threshold, thus a binary result (presence/absence of melt) was derived from the LS-MEMLS liquid water content output (Houtz et al., 2020).

2.2.3 Evaluation method

To assess the surface melt calculation accuracy, we adopted the same formalism and terminology as Colosio et al. (2021), using a confusion matrix with three accuracy metrics: overall accuracy, commission error, and omission error (Table 3). The overall accuracy (Equation 4) is the ratio of correct identifications (positive or negative) to the total number of calculation points; the commission error (Equation 5) is the proportion of incorrect positive melt identifications, i.e., when the algorithm identifies melt but the evaluation data (AWS air temperature or MODIS ice surface temperature) does not; and the omission error (Equation 6) represents the proportion of missed identifications, i.e., when the evaluation data shows melt, but the algorithm result is negative (Tedesco, 2009; Colosio et al., 2021).

$$OA = \frac{TP + TN}{TP + TN + FP + FN}, \tag{4}$$

$$FPR = \frac{FP}{FP + TN}, \tag{5}$$

$$FNR = \frac{FN}{FN + TP}, \tag{6}$$

where *TP*, *TN*, *FP*, and *FN* represent the true positives, true negatives, false positives, and false negatives, respectively; *OA* is the overall accuracy; *FPR* (false positive rate) is the commission error (*CO*); and *FNR* (false negative rate) is the omission error (*OM*).

Table 3 Accuracy evaluation indexes in the confusion matrix formalism

		Actual	
		Not melt	Melt
Projections	Not melt	*TN*	*FN*
	Melt	*FP*	*TP*

To compare surface melt results from MEMLS2 and LS-MEMLS, differences were characterized using the following metrics (Colosio et al., 2021): (1) annual maximum melt range: cumulative sum (over each ablation season) of pixels with positive melt identification as a percentage of the total number of pixels over the Greenland Ice Sheet; (2) daily melt range: daily percentage of pixels with positive melt identification relatively to the total number of ice sheet pixels; (3) mean melt days: ratio of the cumulative sum of melt days for all pixels to the total number of ice sheet pixels.

Surface melt results for both algorithms were compared with surface melt estimates from MODIS surface temperature and AWS air temperature. Because the measurement temporal coverage depends on the observation location and on the meteorological conditions, the number of stations included in the calculations also depends on the year and on the algorithm. During the ablation season, cloud cover over Greenland can affect MODIS measurements, resulting in missing MODIS ice surface temperature data. The MEMLS2 algorithm depends on the availability of DMSP brightness temperature data; because the DMSP microwave radiometers are not sensitive to cloud cover and observe continuously, there were no missing values in the MEMLS2 results. Finally, the LS-MEMLS calculation results depend on the number of available incident angles in the SMOS input data (Houtz et al., 2021). If less than five incident angles were provided, the LS-MEMLS input conditions were not satisfied, resulting in missing LS-MEMLS values (Houtz et al., 2021).

In this study, the number of days with missing values was calculated for each pixel during the ablation season, every year from 2011–2019, for both algorithms and for surface melt estimates from MODIS ice surface temperature measurements (Figure 3). The LS-MEMLS algorithm results (Figure 3a) showed consistently missing data for the same pixels (red arrow, Figure 3a, leftmost panel) every year; there were no missing values in the MEMLS2 algorithm results (Figure 3b); and the MODIS results showed large differences between pixels and between Greenland regions (Figure 3c). For statistical consistency and minimizing the impact of missing values from LS-MEMLS or MODIS on surface melt calculation accuracy, only days and pixels for which data were available simultaneously for MEMLS2, LS-MEMLS, and MODIS were selected.

3 Results and discussion

3.1 Algorithm accuracy evaluation

As explained in Section 2.1.3, in this study, surface melt was estimated from AWS air temperature data for three melt threshold values: 0 °C, –1 °C, and –2 °C, then surface melt results from both algorithms were evaluated separately. Table 4 shows the accuracy for both algorithms, averaged

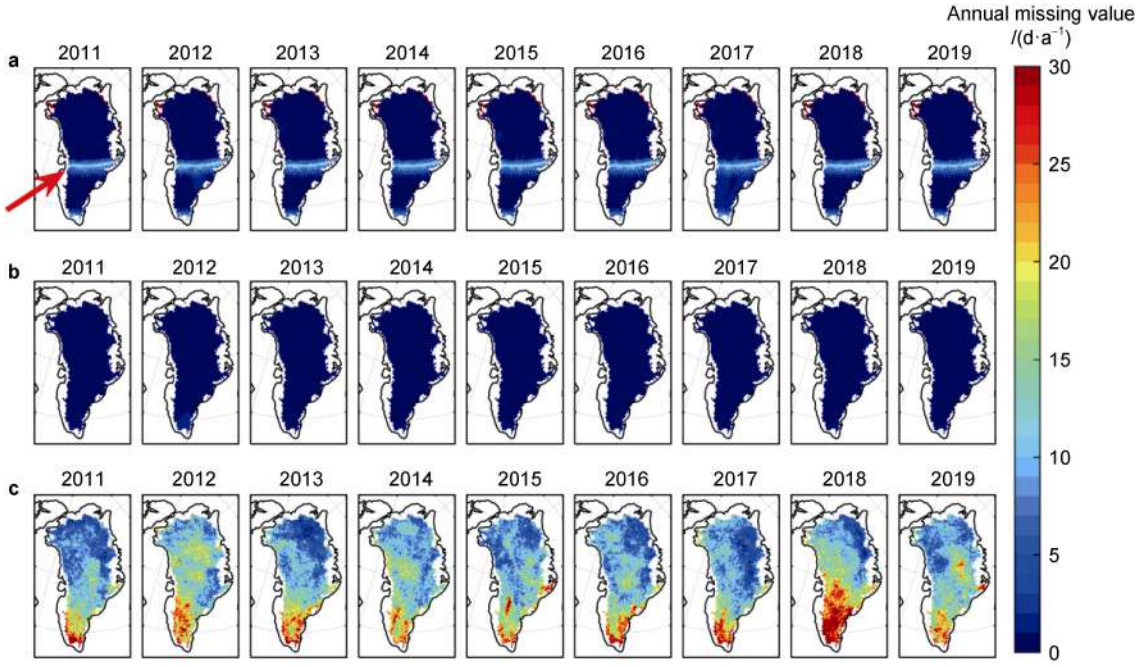

Figure 3 Annual missing value count of surface melt estimates (June–August ablation season, 2011–2019) for LS-MEMLS (**a**), MEMLS2 (**b**, no missing values), and for results derived from MODIS ice surface temperature measurements (**c**).

over all stations and over the complete study period. When the melt threshold decreased from 0 °C to –2 °C, the number of melt days estimated from AWS air temperature remained constant or increased moderately, inducing a possible decrease in the commission error and increase in the omission error. For example, the LS-MEMLS commission and omission errors decreased by 2% and increased by 14%, respectively, for decreasing values of the melt threshold, whereas the commission and omission errors of the MEMLS2 algorithm decreased by 12% and increased by 13%, respectively. Finally, average overall accuracy was 5%–6% higher for MEMLS2 than for LS-MEMLS, independently of the threshold, with consistently lower commission and omission errors for MEMLS2 than for LS-MEMLS.

In this study, global annual averages of the overall accuracy, commission error, and omission error were also calculated over the study period (Table 5) for the three melt thresholds. Highest overall accuracy was calculated for MEMLS2 (87%) in 2011 and 2017, and for LS-MEMLS (84%) in 2017. Conversely, lowest overall accuracy values were 77% in 2020 for MEMLS2 and 70% in 2012 for LS-MEMLS. The interannual trends in the overall accuracy were consistent for both algorithms. Table 5 indeed shows that, in 2011–2020, MEMLS2 overall accuracy is consistently higher, and MEMLS2 commission and omission errors both consistently lower, than those of LS-MEMLS. This indicates that the surface melt simulation performance of the MEMLS2 algorithm is better overall than that of LS-MEMLS.

Table 4 Global averages over the study period (2011–2020) of *OA*, *CO*, and *OM* for LS-MEMLS and MEMLS2 with 0 °C, –1 °C, and –2 °C thresholds

Threshold	LS-MEMLS			MEMLS2		
	OA	*CO*	*OM*	*OA*	*CO*	*OM*
0 °C	77%	36%	31%	82%	23%	18%
–1 °C	78%	35%	38%	84%	17%	23%
–2 °C	79%	34%	45%	84%	11%	31%

Because surface melt estimates from AWS air temperature are only representative of local conditions near a limited number of ground stations, AWS-based results cannot be easily generalized to estimate the global Greenland Ice Sheet surface melt. Therefore, MODIS ice surface temperature data were used in this study to evaluate both algorithms over the complete Greenland Ice Sheet (Figures 4–5). Annual results for both algorithms over Greenland from 2011–2019 are given in Figure 4 for the overall accuracy (Figure 4a), commission error (Figure 4b), and omission error (Figure 4c). Global MEMLS2 overall accuracy is clearly higher than that of LS-MEMLS, whereas the commission and omission errors are both lower than

Table 5 Same conditions as Table 4, but for global annual averages

Year	LS-MEMLS			MEMLS2		
	OA	*CO*	*OM*	*OA*	*CO*	*OM*
2011	74%	33%	40%	87%	15%	17%
2012	70%	37%	40%	82%	18%	15%
2013	82%	19%	46%	83%	10%	31%
2014	80%	27%	43%	81%	13%	40%
2015	79%	32%	52%	84%	14%	29%
2016	78%	32%	40%	86%	16%	18%
2017	84%	33%	36%	87%	17%	30%
2018	81%	31%	39%	86%	17%	26%
2019	74%	57%	28%	80%	24%	22%
2020	74%	51%	30%	77%	28%	22%

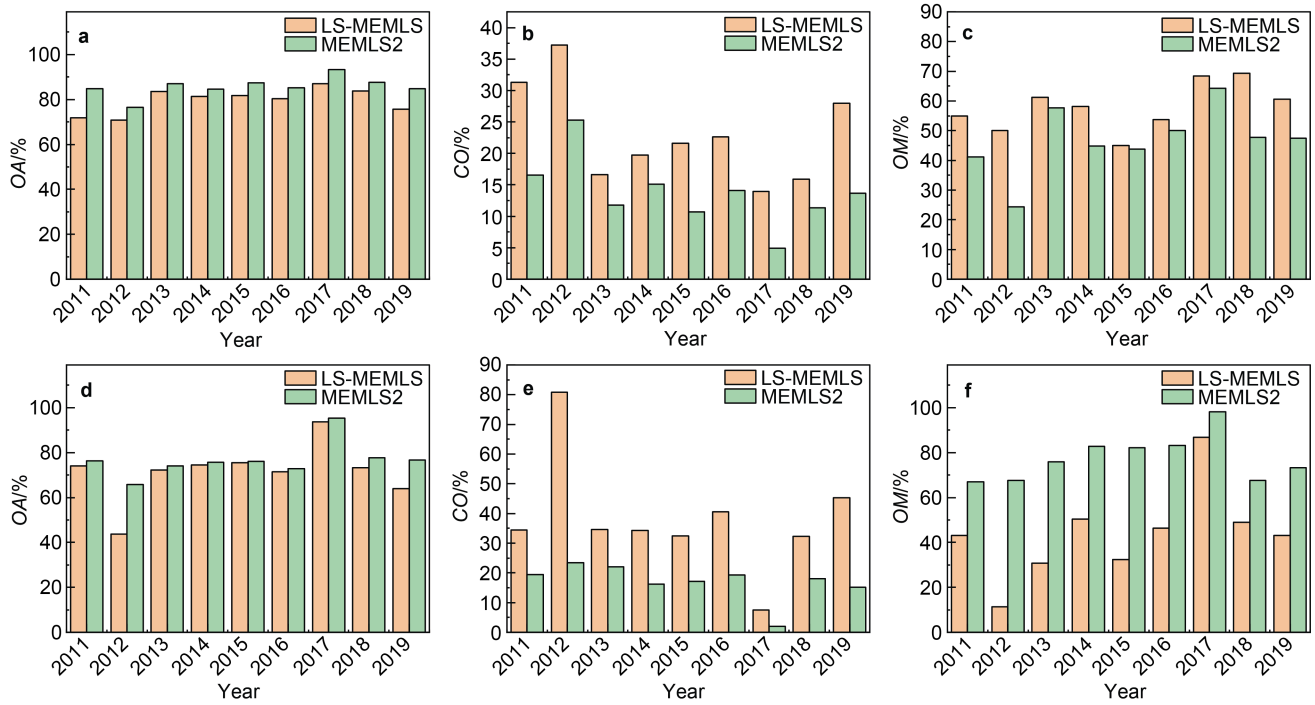

Figure 4 Accuracy assessment for MEMLS2 (green) and LS-MEMLS (orange) by comparison with estimates derived from MODIS ice surface temperature (ablation season, 2011–2019), showing annual averages over the full Greenland Ice Sheet (global, **a**–**c**) and in southeastern Greenland (**d**–**f**) for *OA* (**a**, **d**, respectively), *CO* (**b**, **e**, respectively), and *OM* (**c**, **f**, respectively).

those of LS-MEMLS. This is consistent with the AWS-based evaluation, confirming that MEMLS2 surface melt simulation performance is better than that of LS-MEMLS.

Figure 5 shows the spatial distribution of overall accuracy for both algorithms from 2011–2019. Because missing values were excluded from the comparison, there were no assessment results in a latitude strip with insufficient SMOS incident angles (red arrow, Figure 5, top left panel). In the accumulation zone (inland at high altitudes), surface melt is limited or does not occur. Therefore, both algorithms were expectedly less affected by omission error at high altitudes and their overall accuracy in the accumulation zone was mainly determined by the commission error. As shown in Figure 5, overall accuracy of both algorithms was nearly 100% at high altitudes, also implying low commission error in the accumulation area. Conversely, surface melt and ice sheet mass loss mainly occur in the ablation zone, i.e., the coastal areas (Yang, 2014; Steffen, 2017). Therefore, overall accuracy in the ablation zone depends on both the commission and omission errors. Figure 5 shows markedly lower overall accuracy in the ablation zone than in the accumulation zone, indicating higher commission and omission errors at the

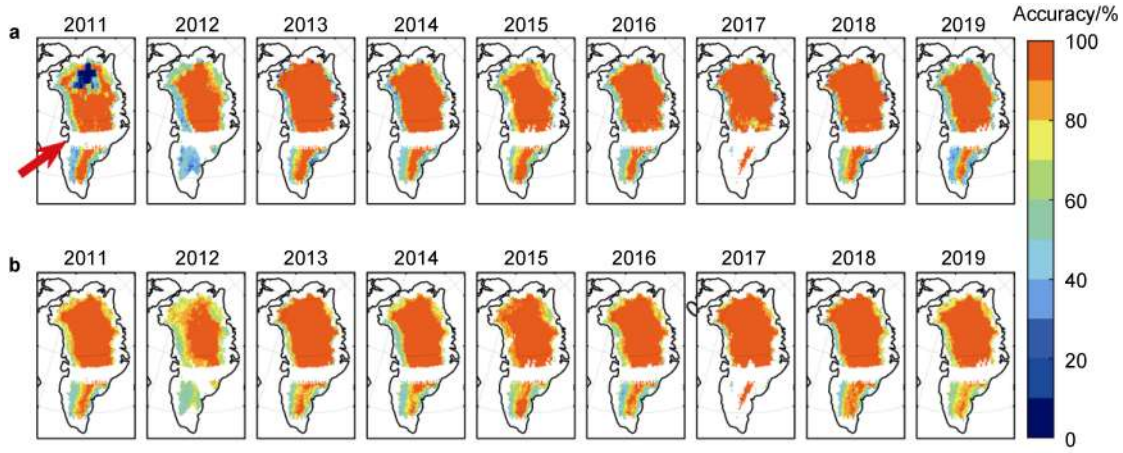

Figure 5 Spatial distribution of *OA* annual averages by comparison with surface melt estimates derived from MODIS ice surface temperature (ablation season, 2011–2019). **a**, Overall accuracy of LS-MEMLS; **b**, Overall accuracy of MEMLS2. The red arrow (top left panel) indicates points excluded from the comparison because of missing LS-MEMLS data.

edge of the Greenland Ice Sheet. Consequently, the MEMLS2 and LS-MEMLS algorithm performance was mainly determined by their results in marginal regions of the Greenland Ice Sheet.

To investigate the spatial distribution of algorithm accuracy, annual averages of the accuracy metrics for MEMLS2 and LS-MEMLS were evaluated separately in each Greenland basin (defined in Figure 2) and at each AWS station, for the 3 melt threshold values (Table 6). Overall accuracy was approximately 90% for both algorithms at high elevation stations such as Humboldt and NEEM (north); NASA-U (northwest); TUNU-N, NASA-E, and EGP (northeast); Saddle (southwest); and South Dome (south). Conversely, overall accuracy was comparatively

Table 6 Same conditions as Table 4, but for basin-wide and station annual averages

Basin	Site	Elevation/m	LS-MEMLS			MEMLS2		
			OA	*CO*	*OM*	*OA*	*CO*	*OM*
North	KPC_U	870	68%	32%	34%	84%	18%	13%
	Peterman ELA	965	41%	3%	71%	58%	13%	45%
	Humboldt	1995	96%	1%	89%	96%	3%	43%
	NEEM	2454	88%	11%	100%	99%	1%	4%
Northwest	UPE_L	220	36%	89%	63%	83%	37%	16%
	UPE_U	940	73%	98%	10%	87%	33%	7%
	CEN	1880	98%	0	100%	99%	0	50%
	GITS	1887	96%	2%	83%	95%	5%	31%
	NASA-U	2369	96%	3%	81%	95%	6%	20%
Northeast	TUNU-N	2113	94%	5%	86%	98%	2%	0
	NASA-E	2631	98%	1%	100%	98%	2%	0
	EGP	2660	99%	1%	100%	99%	0	100%
West-central	Summit	3254	94%	6%	100%	99%	1%	0
Southwest	NUK_U	1120	100%	0	0	82%	34%	14%
	KAN_M	1270	47%	51%	54%	79%	44%	2%
	KAN_U	1840	58%	53%	20%	78%	22%	15%
	DYE-2	2165	74%	30%	26%	87%	13%	15%
	Saddle	2559	88%	12%	53%	90%	10%	8%
Southeast	TAS_L	250	92%	13%	8%	41%	60%	59%
	TAS_U	570	90%	75%	8%	46%	20%	56%
	TAS_A	890	87%	70%	9%	46%	5%	58%
	NASA-SE	2425	61%	8%	86%	58%	3%	83%
South	South Dome	2922	91%	9%	65%	94%	5%	46%

low for low-elevation stations. This confirms that commission and omission error values for both algorithms were mainly calculated at lower elevations, as previously illustrated by the global performance results over Greenland shown in Figure 5.

In terms of commission error, LS-MEMLS yielded consistently higher values than MEMLS2 in all Greenland basins (Table 6). Because the SMOS L-band data are potentially suitable for firn aquifer detection (Houtz et al., 2021), the presence of firn aquifers might have induced an increase in the LS-MEMLS commission error. Shang et al. (2022) mapped the firn aquifer distribution in Greenland from 2010–2020. They inferred that firn aquifers were mainly distributed in northwestern, southwestern, southern, and especially southeastern Greenland, where 88% were distributed below 2000 m and 12% between 2000–2500 m. At the TAS_U and TAS_A stations, the LS-MEMLS commission error calculated in this study was 75% and 70%, respectively, whereas the MEMLS2 commission error was 20% and 5%, respectively. Figure 4e shows the commission error for both algorithms in southeastern Greenland, confirming the markedly higher annual values calculated for LS-MEMLS than for MEMLS2. This indicates that the LS-MEMLS commission error was excessively high in southeastern Greenland, probably because firn aquifers are mainly distributed in that basin.

Finally, we evaluated the contribution of omission error to the LS-MEMLS surface melt simulation performance. As indicated previously, contrary to the MEMLS2 algorithm that only provides binary information on the occurrence or absence of melt, the LS-MEMLS algorithm provides quantitative volumetric information on the liquid water content (Houtz et al., 2021). However, the derived melt occurrence binary result for LS-MEMLS was notably less accurate than MEMLS2 calculations in the southwest of Greenland. This might be explained partly by the sensitivity of SMOS L-band data to supraglacial lakes (Houtz et al., 2021). If a supraglacial lake is deeper than the L-band penetration depth in water, the liquid water volume is underestimated by LS-MEMLS (Houtz et al., 2021), therefore the omission error increases. Hu et al. (2022) identified supraglacial lakes in SAR images throughout Greenland in 2016–2018. They observed that supraglacial lakes were mainly distributed in western and northeastern Greenland, with medium- and large-size lakes mainly in the southwestern and northeastern regions, and that they were mostly present at altitudes of 800–1600 m. Table 6 shows that LS-MEMLS omission error was consistently higher than that of MEMLS2 at low-elevation stations in northern, northwestern, and southwestern Greenland, possibly because of the SMOS L-band sensitivity to supraglacial lakes. In southeastern Greenland, especially at the TAS_L, TAS_U, and TAS_A stations, LS-MEMLS omission error was lower than 10%, whereas MEMLS2 omission error reached 50%. Figure 4f shows the omission error for both algorithms relatively to surface melt estimates from MODIS ice surface temperature in that basin, confirming that the MEMLS2 omission error was markedly higher than that of LS-MEMLS from 2011–2019. In southeastern Greenland, LS-MEMLS exhibited lower omission error, probably because of the scarcity and small size of supraglacial lakes. Conversely, the MEMLS2 algorithm exhibited higher omission error than LS-MEMLS, probably because of excessively high MEMLS2 melt thresholds, inducing omission error increases in that basin.

3.2 Surface melt simulation differences between the algorithms

To compare the simulated surface melt distributions between MEMLS2 and LS-MEMLS, the metrics defined in Section 2.2.3 were calculated over the 2011–2020 study period. The annual maximum melt range is shown in Figure 6. Although there was no previous report of an extreme melt in 2011 (Hall et al., 2013; Colosio et al., 2021), the largest melt range for LS-MEMLS over the study period was detected in 2011 (Figure 6a) and might have been caused by excessive upward substrate brightness temperature noise in 2011 (Houtz et al., 2021). After 2012, the spatial distribution of the LS-MEMLS simulated surface melt did

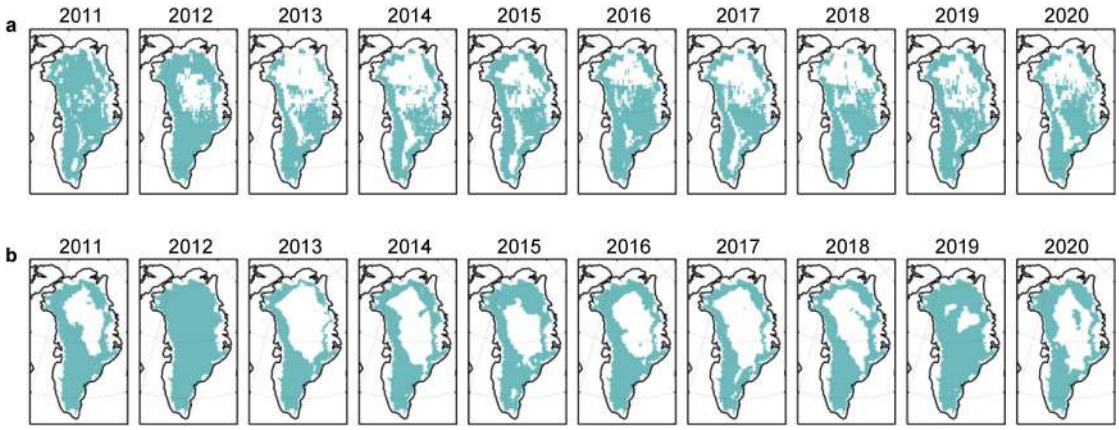

Figure 6 Spatial distribution of the annual maximum melt range (ablation season, full study period). **a**, Annual maximum melt range of LS-MEMLS; **b**, Annual maximum melt range of MEMLS2.

not exhibit marked temporal changes, but melt was also detected in the accumulation area at high elevations. Nghiem et al. (2012) analyzed multisource satellite remote-sensing data and reported a 98.6% melt rate of the Greenland Ice Sheet on 12 July 2012. As shown in Figure 6b, extreme melt was also detected by MEMLS2 in 2012.

As defined in Section 2.2.3, the annual maximum melt range, daily melt range, and annual mean melt days were calculated for both algorithms, during each ablation season, over the study period (Figure 7). Interannual trends of the annual maximum melt range were consistent between the algorithms. In 2012 and 2019, the melt range simulated by LS-MEMLS and MEMLS2 was markedly different (Figure 7a). Additionally, the daily melt range correlation coefficient was low (approximately 0.3), indicating substantial short-timescale simulation differences between the algorithms (Figure 7b). Finally, calculated annual mean melt days and interannual trends were similar for both algorithms, with consistently higher values for LS-MEMLS than for MEMLS2, indicating a longer simulated melt duration for LS-MEMLS than for MEMLS2.

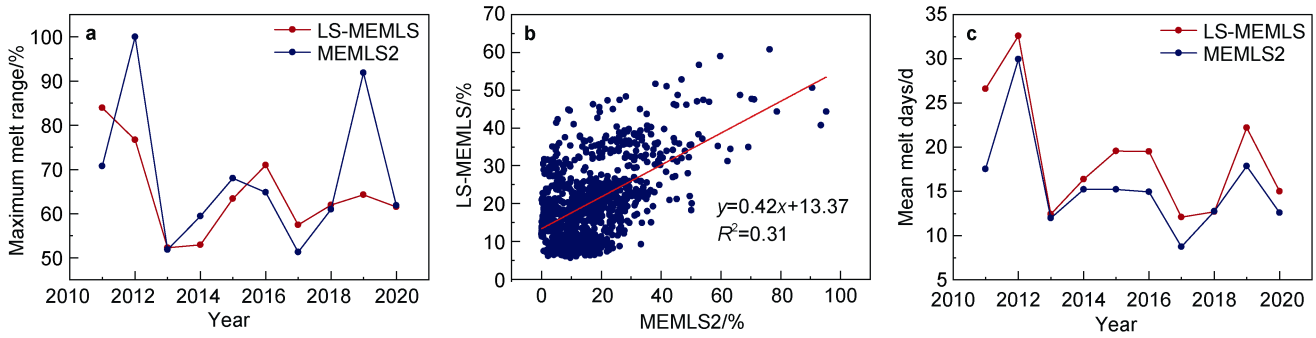

Figure 7 Algorithm cross-comparison (ablation season, full study period) showing: **a**, The temporal variations of the MEMLS2 (blue) and LS-MEMLS (red) annual maximum melt range; **b**, The correlation between the daily melt range results; **c**, The temporal variations of the MEMLS2 (blue) and LS-MEMLS (red) annual mean melt days.

Finally, the spatial distribution of mean melt days during the ablation season, averaged over the study period, was also calculated (Figure 8). In the Greenland margin, long-term melt was detected by MEMLS2 in the southwestern basin, whereas LS-MEMLS detected long-term melt in southeastern and southern Greenland. Supraglacial lakes are mainly distributed in the southwestern part of the Greenland margin (Hu et al., 2022). The presence of supraglacial lakes compromises SMOS L-band measurements, causing LS-MEMLS to underestimate the liquid water content (Houtz et al., 2021). This likely explains the shorter melt times calculated in the southwestern margin by LS-MEMLS. Conversely, firn aquifers are concentrated in southeastern and southern Greenland (Shang et al., 2022). This aquifer presence might correspond to the long-term melt detected by LS-MEMLS, thereby confirming SMOS capabilities for firn aquifer detection.

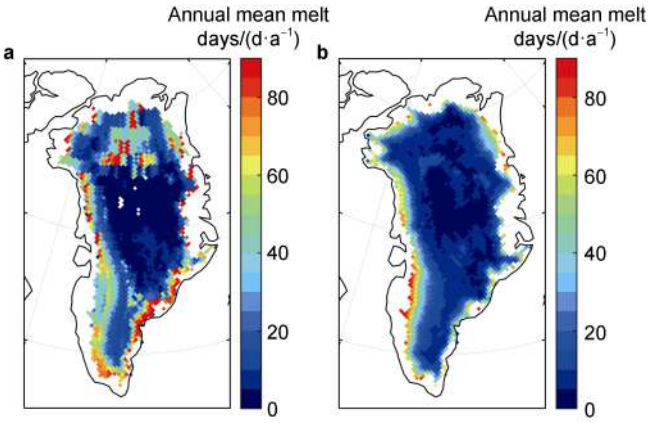

Figure 8 Spatial distribution of the annual mean melt days (ablation season, full study period) for the LS-MEMLS (**a**) and MEMLS2 (**b**) algorithms.

4 Conclusion

In this study, data acquired by microwave radiometer instruments on board the SMOS and DMSP-F17 satellites, with a spatial resolution of 25 km, were used to simulate surface melt on the Greenland Ice Sheet using the MEMLS2 and LS-MEMLS algorithms. First, surface melt estimates derived from AWS air temperature and MODIS ice surface temperature measurements were used as evaluation data to calculate surface melt simulation accuracy for MEMLS2 and LS-MEMLS. Then, surface melt simulations from both algorithms were compared. The following conclusions were drawn from this analysis: (1) Surface melt simulation performance for the complete Greenland Ice Sheet was higher for MEMLS2 than for LS-MEMLS, but MEMLS2 omission error in southeastern Greenland was markedly higher than that of LS-MEMLS, probably indicating poor MEMLS2 applicability in that basin; (2) Because L-band data from SMOS are sensitive to supraglacial lakes and firn aquifers, the LS-MEMLS algorithm was affected by excessive commission and omission errors; thus, DMSP-based surface melt

simulations were more accurate than SMOS-based simulations; (3) Compared with the results of MEMLS2, longer-term surface melts were calculated by LS-MEMLS.

In summary, our study showed that DMSP-based surface melt results were more accurate than SMOS-based simulations, thereby providing a reference for data selection in surface melt studies of the Greenland Ice Sheet. Because of the lack of direct surface melt measurements of the Greenland Ice Sheet, algorithm accuracy was only evaluated by indirect comparison; thus, algorithm accuracy is not fully characterized and remaining error sources might exist. In future studies, developing more suitable surface melt characterization methods could ensure more objective algorithm evaluation and contribute to the development of quantitatively accurate surface melt algorithms.

Data availability statement Data from the Programme for Monitoring of the Greenland Ice Sheet of the Geological Survey of Denmark and Greenland, and from the Greenland Analogue Project, were retrieved from http://www.promice.dk.

Acknowledgments This study was supported by the National Natural Science Foundation of China (Grant no. 42122047), the National Key Research and Development Program of China (Grant no. 2018YFC1406103), and the Basic Fund of the Chinese Academy of Meteorological Science (Grant no. 2021Z006). We appreciate two anonymous reviewers and Guest Editor Dr. Liming Jiang for their constructive comments that have further improved the manuscript.

References

Abdalati W, Steffen K. 1995. Passive microwave-derived snow melt regions on the Greenland Ice Sheet. Geophys Res Lett, 22(7): 787-790, doi:10.1029/95gl00433.

Al Bitar A, Mialon A, Kerr Y H, et al. 2017. The global SMOS Level 3 daily soil moisture and brightness temperature maps. Earth Syst Sci Data, 9(1): 293-315, doi:10.5194/essd-9-293-2017.

Aschraft I S, Long D G. 2006. Comparison of methods for melt detection over Greenland using active and passive microwave measurements. Int J Remote Sens, 27(12): 2469-2488, doi:10.1080/01431160500534465.

Brodzik M J, Long D J, Hardman M A, et al. 2016. MEaSUREs Calibrated Enhanced-Resolution Passive Microwave Daily EASE-Grid 2.0 Brightness Temperature ESDR, Version 1. Boulder, Colorado, USA: NASA National Snow and Ice Data Center Distributed Active Archive Center, doi:10.5067/MEASURES/CRYOSPHERE/NSIDC-0630.001.

Colosio P, Tedesco M, Ranzi R, et al. 2021. Surface melting over the Greenland Ice Sheet derived from enhanced resolution passive microwave brightness temperatures (1979-2019). Cryosphere, 15(6): 2623-2646, doi:10.5194/tc-15-2623-2021.

Flowers G E. 2018. Hydrology and the future of the Greenland Ice Sheet. Nat Commun, 9: 2729, doi:10.1038/s41467-018-05002-0.

Gregory J M, Huybrechts P. 2006. Ice-sheet contributions to future sea-level change. Phil Trans R Soc A, 364(1844): 1709-1732, doi:10.1098/rsta.2006.1796.

Hall D K, Comiso J C, DiGirolamo N E, et al. 2013. Variability in the surface temperature and melt extent of the Greenland Ice Sheet from MODIS. Geophys Res Lett, 40(10): 2114-2120, doi:10.1002/grl.50240.

Hall D K, DiGirolamo N. 2019. Multilayer Greenland Ice Surface Temperature, Surface Albedo, and Water Vapor from MODIS, Version 1. Boulder, Colorado, USA: NASA National Snow and Ice Data Center Distributed Active Archive Center, doi:10.5067/7thuwt9nmpdk.

Houtz D, Naderpour R, Schwank M, et al. 2019. Snow wetness and density retrieved from L-band satellite radiometer observations over a site in the West Greenland ablation zone. Remote Sens Environ, 235: 111361, doi:10.1016/j.rse.2019.111361.

Houtz D, Naderpour R, Schwank M. 2020. Comparison of passive microwave melt detection of Greenland: L-band and XPGR. IGARSS 2020–2020 IEEE International Geoscience and Remote Sensing Symposium. Waikoloa, HI, USA. IEEE, 2983-2986, doi:10.1109/IGARSS39084.2020.9323193.

Houtz D, Mätzler C, Naderpour R, et al. 2021. Quantifying surface melt and liquid water on the Greenland Ice Sheet using L-band radiometry. Remote Sens Environ, 256: 112341, doi:10.1016/j.rse.2021.112341.

Hu J J, Huang H B, Chi Z H, et al. 2022. Distribution and evolution of supraglacial lakes in Greenland during the 2016–2018 melt seasons. Remote Sens, 14(1): 55, doi: 10.3390/rs14010055.

Jay Zwally H, Fiegles S. 1994. Extent and duration of Antarctic surface melting. J Glaciol, 40(136): 463-475, doi:10.3189/s0022143000012338.

Joshi M, Merry C J, Jezek K C, et al. 2001. An edge detection technique to estimate melt duration, season and melt extent on the Greenland Ice Sheet using passive microwave data. Geophys Res Lett, 28(18): 3497-3500, doi:10.1029/2000gl012503.

Liang D, Guo H D, Zhang L, et al. 2021. Time-series snowmelt detection over the Antarctic using Sentinel-1 SAR images on Google Earth Engine. Remote Sens Environ, 256: 112318, doi:10.1016/j.rse.2021.112318.

Nghiem S V, Hall D K, Mote T L, et al. 2012. The extreme melt across the Greenland Ice Sheet in 2012. Geophys Res Lett, 39(20): 2012GL053611, doi:10.1029/2012gl053611.

Rignot E, Box J E, Burgess E, et al. 2008. Mass balance of the Greenland Ice Sheet from 1958 to 2007. Geophys Res Lett, 35(20): L20502, doi:10.1029/2008gl035417.

Shang X Y, Cheng X, Zheng L, et al. 2022. Decadal changes in Greenland Ice Sheet firn aquifers from radar scatterometer. Remote Sens, 14(9): 2134, doi:10.3390/rs14092134.

Smith B, Fricker H A, Gardner A S, et al. 2020. Pervasive ice sheet mass loss reflects competing ocean and atmosphere processes. Science, 368(6496): 1239-1242, doi:10.1126/science.aaz5845.

Steffen K. 2017. Surface energy exchange at the equilibrium line on the Greenland Ice Sheet during onset of melt. Ann Glaciol, 21: 13-18, doi:10.3189/S0260305500015536.

Steffen K, Box J E, Abdalati W. 1996. Greenland Climate Network: GC-Net. CRREL Special Report 96-27, 98-103.

Tedesco M. 2009. Assessment and development of snowmelt retrieval algorithms over Antarctica from K-band spaceborne brightness temperature (1979–2008). Remote Sens Environ, 113(5): 979-997, doi:10.1016/j.rse.2009.01.009.

Tedesco M, Abdalati W, Zwally H J. 2007. Persistent surface snowmelt over Antarctica (1987-2006) from 19.35 GHz brightness temperatures.

Geophys Res Lett, 34(18): L18504, doi:10.1029/2007gl031199.

Torinesi O, Fily M, Genthon C. 2003. Variability and trends of the summer melt period of Antarctic ice margins since 1980 from microwave sensors. J Clim, 16(7): 1047-1060, doi:10.1175/1520-0442(2003) 016<1047: vatots>2.0.co;2.

van den Broeke M R, Enderlin E M, Howat I M, et al. 2016. On the recent contribution of the Greenland Ice Sheet to sea level change. Cryosphere, 10(5): 1933-1946, doi:10.5194/tc-10-1933-2016.

van den Broeke M, Box J, Fettweis X, et al. 2017. Greenland Ice Sheet surface mass loss: recent developments in observation and modeling. Curr Clim Change Rep, 3(4): 345-356, doi:10.1007/s40641-017-0084-8.

Wang X D. 2013. Antarctic ice-sheet freeze-thaw detection based on active and passive microwave remote sensing. Ph. D. thesis, Changsha: Central South University (in Chinese with English abstract).

Yang K. 2014. Understanding Greenland Ice Sheet supraglacial hydrology using a remotely sensed approach. Ph. D. thesis, Nanjing: Nanjing University (in Chinese with English abstract).